Journal of Power Sources 196 (2011) 5829–5834

Contents lists available at ScienceDirect

Journal of Power Sources

journal homepage: www.elsevier.com/locate/jpowsour

Flame synthesis of carbon nanostructures on stainless steel anodes for use in microbial fuel cells

Jennifer L. Lamp[a], Jeremy S. Guest[b], Sayangdev Naha[c], Katherine A. Radavich[d], Nancy G. Love[b], Michael W. Ellis[a,*], Ishwar K. Puri[c]

[a] Department of Mechanical Engineering, Virginia Polytechnic Institute and State University, 100C1 Randolph Hall (MSC 0238), Blacksburg, VA 24061, USA
[b] Department of Civil and Environmental Engineering, University of Michigan, 2340 G.G. Brown Lab, 2350 Hayward Street, Ann Arbor, MI 48109, USA
[c] Department of Engineering Science and Mechanics, Virginia Polytechnic Institute and State University, 225 Norris Hall (0219), Blacksburg, VA 24061, USA
[d] Department of Materials Science and Engineering, University of Wisconsin, Madison, WI 53706, USA

ARTICLE INFO

Article history:
Received 12 January 2011
Received in revised form 25 February 2011
Accepted 28 February 2011
Available online 6 March 2011

Keywords:
Microbial
Fuel cell
Anode
Flame deposition
Carbon nanotubes
Carbon nanofibers

ABSTRACT

Microbial fuel cells (MFCs) offer a promising alternative energy technology, but suffer from low power densities which hinder their practical applicability. In order to improve anodic power density, we deposited carbon nanostructures (CNSs) on an otherwise plain stainless steel mesh (SS-M) anode. Using a flame synthesis method that did not require pretreatment of SS-M substrates, we were able to produce these novel CNS-enhanced SS-M (CNS-M) anodes quickly (in a matter of minutes) and inexpensively, without the added costs of chemical pretreatments. During fed batch experiments with biomass from anaerobic digesters in single-chamber MFCs, the median power densities (based on the projected anodic surface area) were 2.9 mW m^{-2} and 187 mW m^{-2} for MFCs with SS-M and CNS-M anodes, respectively. The addition of CNSs to a plain SS-M anode via flame deposition therefore resulted in a 60-fold increase in the median power production. The combination of CNSs and metallic current collectors holds considerable promise for power production in MFCs.

1. Introduction

Microbial fuel cells (MFCs) are devices that use microorganisms to generate current from biologically mediated oxidation or reduction reactions [1]. Electricity production via oxidation reactions is achieved by exoelectrogens, microorganisms capable of extracellular electron transfer [2]. There are a wide range of potential applications for MFCs including their use as sea floor batteries [3], as power sources for wireless sensors [4], in the treatment of high-strength wastewaters [5], and as biosensors to monitor organic carbon concentrations in wastewater [6]. Significant challenges facing MFCs include the need for a continued reduction in electrode material cost and for increased current densities (based on electrode surface area) [7].

In order to harness electricity from biologically mediated oxidation reactions, electrons must be conveyed to the electrode surface. The amount of anodic surface area and its ability to support biofilm formation, therefore, are key contributors to MFC performance [2]. A number of efforts have been made to improve anodic properties, including both physical and chemical modifications to traditional, carbon-based electrode materials [8–10]. An emerging research area is the use of carbon nanostructures (CNSs) to enhance MFC anode properties. In particular, carbon nanotubes (CNTs) have received significant attention in fuel cell research for their unique structural and conductive properties [11]. Nanostructure attachment to electrode backbones has been achieved through the use of conductive polymers [12,13] or by allowing for evaporation of the carrier solution [14,15]. Improvements in anodic power density have been observed following the addition of CNTs [15,16], but most deposition strategies rely on the use of harsh chemicals and take a number of hours [15] or days [12–14] from start to finish; a time-scale that is not conducive to the economical production of MFC anodes.

Alternatively, flame synthesis is a rapid and scalable process that can be used to synthesize a range of CNSs including single-walled CNTs [17], multi-walled CNTs (MWNTs) [18,19], carbon nanofibers [18,20], carbon nodules [21], and carbon nanobeads [22] in a matter of minutes [17,21]. Particularly relevant to MFCs are past reports of CNS flame synthesis on stainless steel without any pretreatment or modification [20,21]. Stainless steel is highly durable, conductive, commercially available and widely used in corrosive environments, but has met with mixed results in its use as a MFC anode [23,24]. However, due to its distinct advantages as an efficient current col-

* Corresponding author. Tel.: +1 540 231 9102; fax: +1 540 231 9100.
E-mail addresses: jenlamp@bu.edu (J.L. Lamp), jsguest@umich.edu (J.S. Guest), sayangdev@gmail.com (S. Naha), kradavich@gmail.com (K.A. Radavich), nglove@umich.edu (N.G. Love), mwellis@vt.edu (M.W. Ellis), ikpuri@vt.edu (I.K. Puri).

0378-7753/$ – see front matter © 2011 Elsevier B.V. All rights reserved.
doi:10.1016/j.jpowsour.2011.02.077

Fig. 1. Co-flow axisymmetric burner used for flame synthesis of CNSs.

lector and durable material, researchers are not prepared to dismiss the use of stainless steel as a component of MFC anodes [7,24].

Although carbon and graphite do possess a number of excellent properties as anode materials, they are brittle and have conductivities that are often three orders of magnitude lower than metals [25]. Therefore, the use of durable metallic backbones combined with a thin layer of CNSs could offer exciting opportunities in the advancement of MFC anode design [25]. In this study, CNSs were flame synthesized on stainless steel mesh anodes to evaluate their impact on anodic power density in MFCs. The complete anode modification took 15 min and required no pretreatment of the stainless steel. All biological MFC experiments were inoculated with biomass from anaerobic digesters and operated in fed batch mode. Bare and CNS-enhanced stainless steel anodes were run side-by-side using single-chamber MFCs and evaluated based on power production at a constant voltage with a potentiostat.

2. Materials and methods

2.1. Anode fabrication and characterization

The base anode material for all experiments was stainless steel mesh (type 304, woven wire diameter 0.016 inch, 20 × 20 openings per square inch; Small Parts, Inc.; Miami Lakes, FL). Stainless steel mesh was used as received (without pretreatment; SS-M) or modified via flame synthesis of carbon nanostructures (CNS-M). All meshes were cut into 2.54 cm squares (projected surface area of 6.45 cm^2). Flame synthesis of CNSs was achieved using a co-flow axisymmetric burner. As illustrated in Fig. 1 (described in more detail in [21]), the burner consisted of two coannular tubes delivering a non-premixed flame – the inner tube for ethylene fuel flow with a diameter of 11.1 mm and the outer tube for air flow with a diameter of 101.6 mm. This burner produced a steady laminar flame with flow rates of ethylene and air of 0.276 ± 0.007 L min^{-1} and 34.7 ± 0.2 L min^{-1}, respectively. The stainless steel surfaces were mounted in a clamp, 5 mm above the base of the non-premixed flame for 3 min. At this location, the flame temperature is on the order of 1550 °C [19] and CNS formation has been previously observed [20,21]. The carbon nanostructures are primarily formed in the toroidal flamefront zone where the concentration of carbon monoxide is maximum since the pyrolyzed fuel is partially oxidized. The stainless steel metal catalyst appears to be preferentially more reactive towards carbon monoxide as opposed to the ethylene. The low soot fraction in this region [26] also prevents active sites from being poisoned. The carbon in the carbon monoxide is adsorbed onto the metal catalytic surface. Once enough carbon is adsorbed on a catalyst nanoparticle, nucleation occurs, leading to carbon precipitation in the form of the carbon nanostructures [27–29]. Methods to control feature size and distribution of the carbon nanostructures [30] include varying the (i) temperature, e.g., by diluting the flame with a nitrogen flow, (ii) amount of carbon dioxide, e.g., by changing the stoichiometry or using a partially premixed flame [31], or the (iii) the fuel by altering the numbers of unsaturated carbon atoms in it [32].

Imaging of anodes was achieved using a FEI Quanta 600 FEG environmental scanning electron microscope (E-SEM). Images of anodes before placement in MFCs were taken using the 'high-vacuum' E-SEM mode (up to 10^{-5} Torr) while images of anodes after placement in a MFC were taken using the 'low-vacuum' mode (0.8 Torr). Nitrogen adsorption–desorption experiments were conducted at 77 K in the range of 0.05–1.00 P/P_0 with a NOVA 4200e (Quantachrome Instruments; Boynton Beach, FL) running version 9.0 of the NovaWin2 software package. Ultra-high purity N_2 (99.999%; Cryogenic Gases, Inc.; Detroit, MI) was used as received. Specific surface areas ($cm^2\ g^{-1}$) and pore volume distributions were calculated using the Brunauer–Emmett–Teller (BET) and Barrett–Joyner–Halenda (BJH) methods, respectively. All samples were degassed at 300 °C for 2 h prior to analysis. Due to the very low surface area to mass ratio of SS-M anodes, these samples could not be characterized with BET or BJH. Instead, specific surface area was estimated based on the known wire diameter and an assumed density of 8.0 g cm^{-3}.

2.2. MFC configuration and performance evaluation

Experiments were conducted using four to six identical, single-chamber, open-air cathode MFCs. The end plates, sampling ports, and cylindrical chamber of each MFC were polycarbonate and the assembly had a final volume of 142 mL. The cathode membrane electrode assembly (MEA) consisted of a Nafion® 117 membrane (Ion Power, Inc.; New Castle, DE) coated only on the air-facing side with a 20 cm^2 catalyst layer comprised of approximately 30 (w/w) Nafion® DE521 solution (Ion Power, Inc.) and carbon supported platinum catalyst (39.1% Pt on Vulcan XC-72; E-TEK; Somerset, NJ), yielding a platinum loading of approximately 0.4 mg cm^{-2}. A woven gas diffusion layer (HT 2500-W; E-TEK) was placed between the cathode MEA and a slotted stainless steel conducting plate. Anodes (either SS-M or CNS-M) were clamped between bolts on a threaded stainless steel supporting rod and positioned 2.0 cm from the cathode.

MFC performance was evaluated using a potentiostat (Solartron 1480 MultiStat) with Corrware software. Open circuit voltage (OCV) was measured and a polarization curve was generated for each MFC by running a potentiodynamic test consisting of a voltage sweep at 5 mV s^{-1} from the OCV to a voltage of 0.1 V or less. Potentiostatic tests were conducted at roughly half the average OCV of the MFCs (0.25 V for all biological experiments). Biological fed batch experiments lasted 7–12 days with current production data recorded every 20–100 s. Power densities are reported based on the projected surface area of all anodes (6.45 cm^2) unless otherwise stated. Electrochemical impedance spectroscopy (EIS) was performed on MFCs with sterile media in duplicate for each anode material to determine the high frequency resistance of the cell.

2.3. Media

A predefined phosphate buffered medium [33] was used, modified to contain 1.0 g L^{-1} glucose in place of sucrose. The media

consisted of the following (per liter of distilled and deionized water, ASTM type I): glucose (1.0 g), NH_4Cl (0.2 g), $CaCl_2{\cdot}2H_2O$ (0.15 g), KCl (0.33 g), NaCl (0.3 g), $MgCl_2$ (3.15 g), K_2HPO_4 (1.26 g), KH_2PO_4 (0.42 g), yeast extract (0.25 g), and trace metals (1 mL [34]). Media (without glucose) was autoclaved, then supplemented with a glucose stock solution that was filter sterilized through a 0.2 μm polyvinylidene fluoride (PVDF) filter and stored at 4 °C. The final media solution was pH adjusted to 7.5 with filter sterilized (through a 0.2 μm nylon syringe filter) 50% (w/w) sodium hydroxide immediately preceding fed batch experiments. To reduce the dissolved oxygen concentration, media was bubbled for 30 min with 99.6% N_2 gas routed through a 0.22 μm HEPA® filter.

2.4. Fed batch experiments

Prior to all experiments, MFC components (except the MEA) were wiped liberally with or dipped in (in the case of the anodes) 70% ethanol and assembled using aseptic techniques. As the highest power densities have been achieved with rich and diverse cultures of bacteria [2], MFCs in biological runs were inoculated with biomass from a thermophilic laboratory-scale reactor or from mesophilic full-scale anaerobic digesters treating municipal wastewater solids. MFCs were continuously mixed with a magnetic stir bar and spiked with 500 mg L^{-1} glucose every 2 days. The pH was monitored daily during biological experiments and adjusted to remain between 7.0 and 8.5 with sodium bicarbonate (86 g L^{-1}). Three independent biological runs with SS-M and CNS-M MFCs run side-by-side (twice in duplicate, once in triplicate) were achieved, totaling seven true replicates per anode type. New anodes were used in every experiment and all MFCs were cleaned and sterilized between biological runs.

In addition to biological experiments, abiotic (two independent runs, four total replicates per anode type) and biologically inhibited (discussed below) controls were also performed to confirm electricity production was biologically mediated. The inhibition experiment was conducted as one event with four MFCs, all with CNS-M anodes. After 5 days of fed batch operation, power production began to steeply increase. At this time, sodium azide (NaN_3, a respiratory inhibitor) was added to two of the four MFCs to reach a final concentration of 10 mM. Although azide may not be appropriate for complete inactivation of all relevant anaerobes [35], it has been shown to inhibit some forms of anaerobic respiration [36] including glucose fermentation [37]. This experiment allowed us to observe the effect of biological inhibition on power production.

3. Results

3.1. EIS with SS-M and CNS-M anodes

EIS measurements were used to determine the high frequency resistance (HFR) of the MFC (including both electrical and ion transport resistances) containing sterile media in duplicate for each anode type. The average values of HFR for MFCs with SS-M and CNS-M anodes are approximately 22 Ω and 18 Ω, respectively. These values are not significantly different ($P = 0.51$, based on an unpaired, two-tailed t-test) as expected, given that the same media and hardware was used in each MFC.

3.2. Electricity production with SS-M and CNS-M anodes

Maximum power production was determined using a 2-h moving average. Seven and nine biological runs were achieved with SS-M and CNS-M anodes, respectively, over the course of four separate fed-batch experiments (Table A.2). (Note: CNS-M results include the two uninhibited controls from the inhibition experiment.) Although maximum power production by MFCs varied

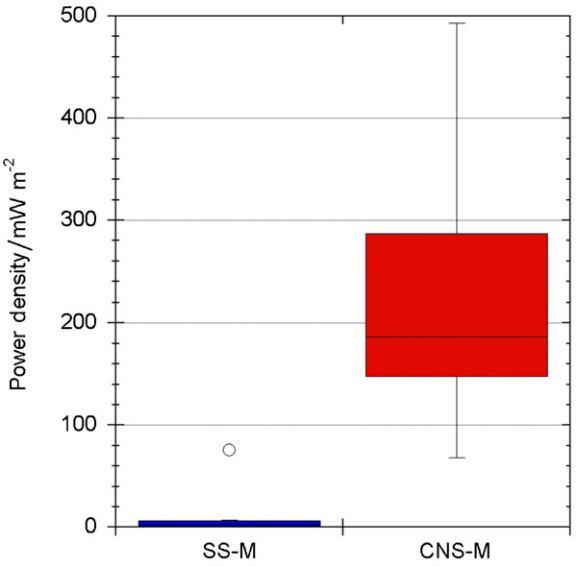

Fig. 2. Box and whisker plot of MFC anodic power densities for fed batch experiments with SS-M and CNS-M anodes. The colored boxes represent the span of the lower (25th percentile) and upper (75th percentile) quartiles of seven and nine replicates for SS-M and CNS-M anodes, respectively. The horizontal line within each box represents the median, and the vertical lines ("whiskers") represent the span of the data, excluding the outliers (of which there is one, represented as a circle in the SS-M data). Details regarding outlier identification can be found in Appendix A.

across fed-batch experiments (partially due to the inocula), a comparison of biological power production with the two types of anodes revealed that CNS-enhanced anodes increased power production (Fig. 2). Based on a projected anode area of 6.45 cm^2, SS-M anodes achieved a median power production of 3.0 mW m^{-2} while CNS-M anodes achieved a median of 187 mW m^{-2}. Maximum observed power productions (2-h average) were 75 and 493 mW m^{-2} for SS-M and CNS-M anodes, respectively.

Although the aseptic techniques limited the initial concentration of microorganisms in the abiotic experiments, the lack of MEA sterilization meant the MFCs were not completely abiotic. However, the techniques were sufficient to limit the microbial density to a small fraction of the density used during biotic experiments and the CNS-M abiotic controls confirmed that the media was not responsible for appreciable power production (data provided in Table A.1 provided in the Appendix). Abiotic tests also revealed, that SS-M anodes did not facilitate appreciable biologically mediated power production. Comparison of abiotic and biological runs with SS-M anodes revealed that the addition of microorganisms to the MFCs did not increase power production with statistical significance ($P = 0.12$ based on a single factor ANOVA). Greater variability was also seen in the OCV of SS-M MFCs (0.44 ± 0.19 V) as compared to CNS-M MFCs (0.40 ± 0.08 V). Differences in anode OCV values were not statistically significant ($P = 0.55$ based on an unpaired, two-tailed t-test). The observation of similar OCV values for the SS-M and CNS-M anodes, despite the large difference in power, is attributable to the small biofilm growth on the SS-M anodes, which was able to produce an electrochemical potential but not of sufficient mass to produce current (and power) comparable to the CNS-M anodes. Other research has also shown that power density may be quite different despite similar OCV (e.g. [9]).

The inhibition experiment with CNS-M anodes provided additional evidence that power production was biologically mediated (Figure A.1, Appendix). After the addition of sodium azide to two MFCs, uninhibited MFCs continued to produce electricity while inhibited reactors experienced a drastic decrease in activity.

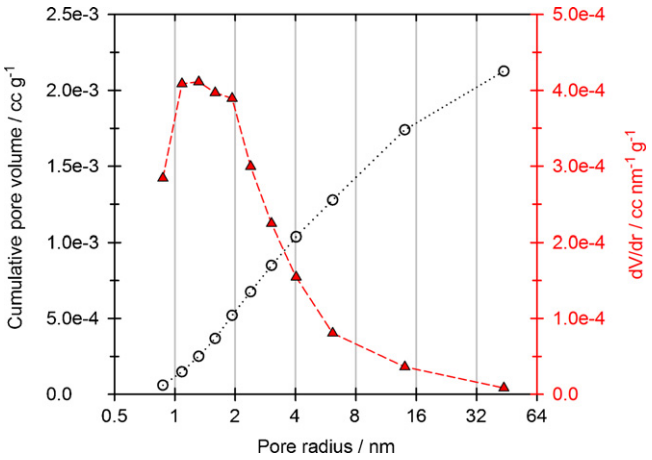

Fig. 3. Cumulative pore volume (open circles, left axis) and derivative of cumulative pore volume (filled triangles, right axis) of CNS-M anode (post-ethanol dip) using BJH method.

3.3. CNS-M anode characteristics

CNSs successfully formed on the stainless steel mesh (without the use of a separate catalyst) in non-uniform clusters that were visible via scanning electron microscopy. Previous results have elucidated the mechanism of CNS formation [27–29] and have shown these nanostructures to be completely graphitic containing encapsulated metal particles [20].

For a projected anode area of 6.45 cm^2, surface area analysis indicated an increase in anode surface area from 9.83 cm^2 for bare stainless steel mesh (calculated) to 17,500 ± 3300 cm^2 after CNS-enhancement (CNS-M BET results based on average of 2 full anodes, ±half the difference between measurements) – a surface area increase of roughly 1800 times. In order to run abiotic controls, however, the anodes were dipped in 70% ethanol (this was done prior to all experiments for consistency). This sterilization procedure resulted in a loss of some CNSs, and was observed to reduce CNS-M surface area to 3100 cm^2 (based on a single BET result using 3 full anodes) and decrease surface carbon content (measured via energy dispersive spectroscopy; data not shown). The CNS-M anodes (post-ethanol treatment) used in experimentation, therefore, had a surface area roughly 300 times larger than SS-M anodes. BJH results (post-ethanol treatment) show that approximately half of the pore volume is contained within pores smaller than 4 nm (Fig. 3) – more than two orders of magnitude smaller than the cells themselves. Although there are multiple mechanisms for extracellular electron transfer [2], it is unclear whether or not these pores are bioavailable.

3.4. Microorganism attachment to CNS-M anodes

Fig. 4 presents representative images of SS-M and CNS-M anodes before and after a fed batch run. Fig. 4A and D show portions of SS-M and CNS-M anodes, respectively, before being placed in MFCs. Magnified images of these surfaces show visible clusters of flame-deposited CNSs on the CNS-M anode (Fig. 4E) and the contrasting plain stainless steel surface of the SS-M anode (Fig. 4B). Fig. 4F shows biomass attached to the surface of a CNS-M anode, which is in contrast to Fig. 4C, where significantly less biomass attachment is visible on the SS-M anode. A high resolution E-SEM image of biomass attachment to a CNS-M anode can be seen in Fig. 5.

4. Discussion

4.1. Microorganism attachment to CNS-M anodes

It is likely that the surface residue observed on the anodes in each of the experiments is a mixture of microorganisms and extracellular polymeric substance (EPS) excreted by the microorganisms. Amorphous carbon films and CNTs provide hydrophobic

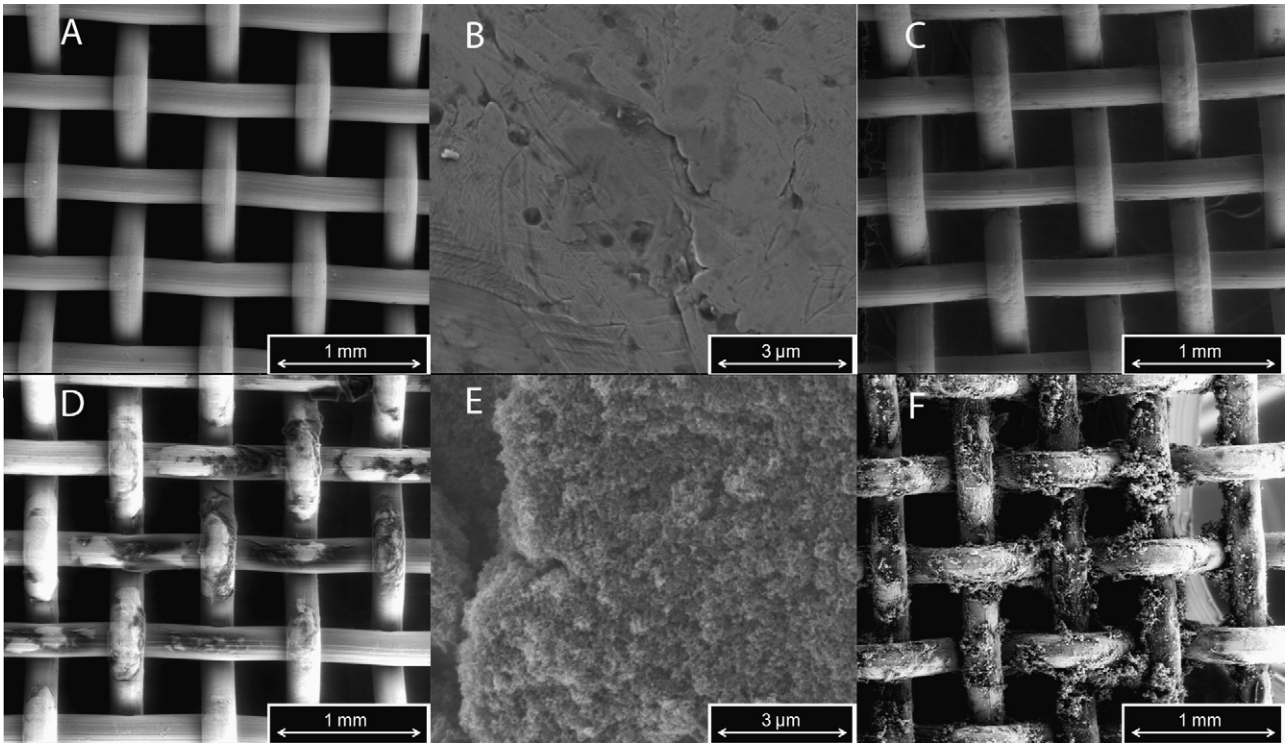

Fig. 4. E-SEM images of SS-M (A, B, C) and CNS-M (D, E, F) anodes. Images were taken before exposure to biomass at low (A and D) and high (B and E) resolutions, and after exposure to biomass (C and F).

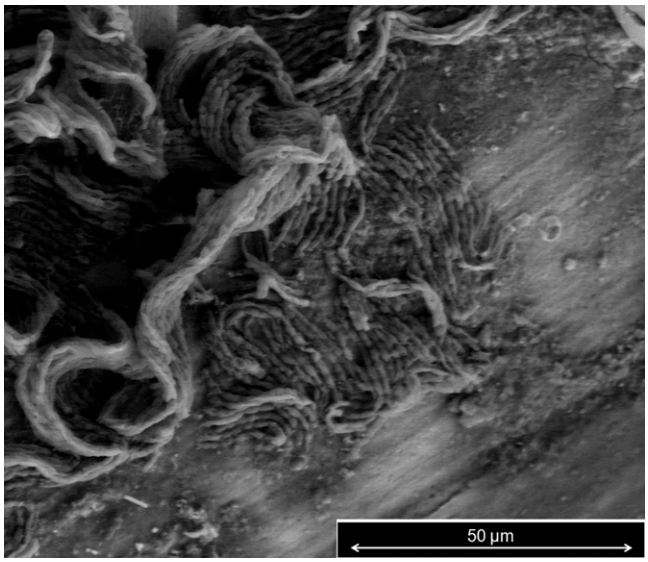

Fig. 5. E-SEM image of microbial attachment to a CNS-M anode after a fed batch experiment.

surfaces [22,38,39] which have been shown to support cell attachment and growth by *Mycobacterium* [40] and neuronal cells [41]. Hydrophobic binding may also enhance biomass attachment with the CNS-enhanced anodes. The reduction in surface area due to the immersion of CNS-M anodes in ethanol (17,500 cm^2 to 3100 cm^2) indicates that perhaps the use of other sterilization methods (or the absence of sterilization) may allow for an even larger increase in power production in MFCs with CNS-enhanced anodes.

4.2. Comparison to previous anodic modification studies

Anodic CNS modification is a relatively new field of research. Similar to the results presented here, several studies have noted large improvements in MFC power density following the addition of CNTs to the anode. Qiao and colleagues, for example, observed significant increases in anodic power density (maximum power density = 42 mW m^{-2}) using *Escherichia coli* K-12 cultures and nickel foam anodes coated with CNT-polyaniline (PANI) paste [12]. Carbon paper anodes have also been sprayed with polypyrrole-coated carbon nanotubes (PPy-CNTs) and achieved a maximum power density of 228 mW m^{-2} at a loading of 5 mg cm^{-2} PPy-CNTs [13]. Tsai and colleagues observed a greater than 2-fold increase in anodic power density, from 26 to 65 mW m^{-2}, of carbon cloth anodes after chemically pretreated MWNTs were applied [15]. More recently, Sun and colleagues synthesized MWNTs directly on carbon paper utilizing layer-by-layer (LBL) assembly resulting in a power density of 290 mW m^{-2}, a 20% increase compared to the bare carbon paper anode [16]. Our maximum anodic power density (based on projected surface area) was 493 mW m^{-2} and is one of the highest achieved using anodes enhanced with CNSs. It should be noted, however, that the broader literature (including anodes not enhanced by CNS) reflects an even wider range of performance. Among the highest values reported for power density, were cells reported by Cheng, Liu, and Logan in which performance for carbon paper anodes ranged from 300 to 1200 mW m^{-2} for acetate feed [42,43] and performance for carbon cloth anodes was 766 mW m^{-2} with glucose feed [44]. In non-planar geometries, power density values for graphite fiber brushes have been reported as high as 2400 mW m^{-2} [45] and for carbon granule reactors have been reported as 460 mW m^{-2} [46], 660 mW m^{-2} [47], and 1800 mW m^{-2} [48] where in each case, we have normalized to the area of the interface with the cathode to allow comparison with planar MFCs. The difficulty in choosing an appropriate area for normalization complicates comparisons between planar geometries and non-planar geometries (e.g., brush and granule designs). Further complicating comparisons of MFC performance are the wide range of microorganisms (including pure and diverse cultures), the nature of the feed, cell geometry and a variety of other factors. Thus, while the CNS enhancement clearly improved anode performance over the SS-M baseline, additional research is required to establish the benefits of CNS enhanced stainless steel with respect to other anode material options.

4.3. Benefits and potential of flame-synthesized CNSs on MFC anodes

Using an inexpensive flame synthesis method without pretreatment, our anodic power densities increased significantly using CNS-enhanced anodes. Flame synthesis has been shown to form CNSs on timescales of minutes [21] with CNTs having been observed within tens of milliseconds [17]. In contrast, LBL assembly can take over half an hour for each layer [16,49], chemical pretreatment can require hours [15] or days [14], and the synthesis of PPy-CNTs and CNT-PANI composites takes days from start to finish [12,13]. Synthesis of CNSs does require a catalyst, but transition metals (e.g., Fe) and their alloys have been proven to serve as sites for CNS formation [20,50]. Thus, the use of stainless steel as the anode substrate has the advantage of generating catalyst particles directly from the substrate without the need for pretreatment, eliminating the cost of chemical additives. In assessing the overall cost of CNS enhanced anodes, the cost of stainless steel (approximately \$4 kg^{-1}, \$0.03 cm^{-3} for 304ss [51]) must be compared with the cost of alternative materials such as carbon fiber (approximately \$10 kg^{-1}, \$0.02 cm^{-3} [51]) in the context of the specific geometric and structural requirements of the MFC.

Additional studies into the use of flame deposition as a method to create CNS-coated anodes could lead to further improvements in the efficiency of CNS-M anode production and anodic power densities of MFCs. In our current system (Fig. 1), there are no CNSs located at the very center of the ethylene-air flame [20]. Improvements to the manufacturing process may, therefore, further increase the speed and efficiency of CNS-enhancement of anode materials. Also, the hydrophobicity of CNSs has been shown to change with time in the flame [21], so biofilm growth on the anode could be optimized by altering the length of CNS deposition time, leading to further increases in MFC power densities. Another area for further development is the improvement of CNS retention on the SS surface. The ethanol rinse used to sterilize the anodes for the pseudo-sterile experiments was found to remove significant amounts of CNS material. While typical operating conditions would not expose the anode CNSs to such high concentrations of ethanol, other wastewater chemicals and operating conditions could lead to loss of CNS material. Studies of flame synthesized CNSs have shown that a variety of processing variables (e.g., flame configurations, fuel types, and catalytic materials [52]) affect CNS features such as geometry, characteristic length, entanglement, and substrate interaction. Further development of a CNS modified anode should address the connection between these features and CNS retention and explore the optimization of process variables to improve attachment.

Finally, the effect of CNS pore size on power density should be explored. Although specific surface area and pore volume distribution data were collected, it is unclear what portion of the surface area is actually accessible to the microorganisms, which are larger than most of the anode pores. The cells themselves are much larger than most of the anode pores, and even bacterial nanowires (50–150 nm in diameter [53]) are still an order of magnitude larger than many of the pores on the anode surface. Of the known mechanisms for extracellular electron transport [2], the use of soluble

redox mediators may be the only way for cells to deposit electrons within smaller nanostructure pores (e.g., pores smaller than 4 nm). The bacterial production of soluble electron shuttles has been observed to significantly increase electron transfer in MFCs, and it has been argued that these mediators may allow for transfer of electrons through multi-layer biofilms to an anodic substratum [54]. We speculate, therefore, that soluble electron shuttles may also increase the accessible surface area of meso- and microporous anodes. Additionally, it is likely that micrometer-scale structures and nanometer-scale roughness facilitated the attachment of cells to the anode.

4.4. Summary

Flame synthesis can achieve continuous, energy-efficient CNS deposition in a matter of minutes [21] without expensive starting material [17]. In this study, CNSs were applied to highly conductive stainless steel mesh anodes in an effort to improve anode power densities in microbial fuel cells using a fast and inexpensive flame-deposition method. We have shown that a significant increase in power density can be achieved using this new anode treatment when compared to uncoated stainless steel mesh anodes. The maximum anodic power density achieved was 493 mW m^{-2} (based on projected surface area), which is one of the highest reported for CNS-modified anodes. Although it is clear that the electricity produced was biologically mediated, the exact mechanism causing the increase in power density is unknown. Ultimately, CNS-enhancement of highly conductive current collectors offers an exciting opportunity for MFC anode enhancement.

Acknowledgements

Jennifer Lamp and Jeremy Guest contributed equally to this work. This work was supported by the Institute for Critical Technology and Applied Science (ICTAS) at Virginia Tech (Michael Ellis, Principal Investigator), the Water Environment Research Foundation (WERF) project ID U1R06 (Nancy Love, Principal Investigator), and the National Science Foundation (NSF) award number EEC-0552738. The authors would like to thank Joshua Sole, Ross Frey, Zachary Frye, and Thomas Cochell for their contributions preceding the work presented here. Parts of this work were carried out using instruments in the Nanoscale Characterization and Fabrication Laboratory operated by ICTAS with the help of Steve McCartney (E-SEM), and the Microporous Materials Characterization Laboratory (University of Michigan) with the help of Antek Wong-Foy (NOVA 4200e). Any opinions, findings, and conclusions or recommendations expressed in this material are those of the author(s) and do not necessarily reflect the views of the National Science Foundation or the Water Environment Research Foundation.

Appendix A. Supplementary data

Supplementary data associated with this article can be found, in the online version, at doi:10.1016/j.jpowsour.2011.02.077.

References

[1] K. Rabaey, J. Rodriguez, L.L. Blackall, J. Keller, P. Gross, D. Batstone, W. Verstraete, K.H. Nealson, ISME J. 1 (2007) 9–18.
[2] B.E. Logan, Nat. Rev. Microbiol. 7 (2009) 375–381.
[3] L.M. Tender, C.E. Reimers, H.A. Stecher, D.E. Holmes, D.R. Bond, D.A. Lowy, K. Pilobello, S.J. Fertig, D.R. Lovley, Nat. Biotechnol. 20 (2002) 821–825.
[4] A. Shantaram, H. Beyenal, R. Raajan, A. Veluchamy, Z. Lewandowski, Environ. Sci. Technol. 39 (2005) 5037–5042.
[5] P. Aelterman, K. Rabaey, P. Clauwaert, W. Verstraete, Water Sci. Technol. 54 (2006) 9–15.
[6] M. Di Lorenzo, T.P. Curtis, I.M. Head, K. Scott, Water Res. 43 (2009) 3145–3154.
[7] B.E. Logan, Appl. Microbiol. Biotechnol. 85 (2010) 1665–1671.
[8] B.E. Logan, B. Hamelers, R. Rozendal, U. Schroder, J. Keller, S. Freguia, P. Aelterman, W. Verstraete, K. Rabaey, Environ. Sci. Technol. 40 (2006) 5181–5192.
[9] X. Wang, S.A. Cheng, Y.J. Feng, M.D. Merrill, T. Saito, B.E. Logan, Environ. Sci. Technol. 43 (2009) 6870–6874.
[10] Y.J. Feng, Q. Yang, X. Wang, B.E. Logan, J. Power Sources 195 (2010) 1841–1844.
[11] H.S. Liu, C.J. Song, L. Zhang, J.J. Zhang, H.J. Wang, D.P. Wilkinson, J. Power Sources 155 (2006) 95–110.
[12] Y. Qiao, C.M. Li, S.J. Bao, Q.L. Bao, J. Power Sources 170 (2007) 79–84.
[13] Y.J. Zou, C.L. Xiang, L.N. Yang, L.X. Sun, F. Xu, Z. Cao, Int. J. Hydrogen Energy 33 (2008) 4856–4862.
[14] L. Peng, S.J. You, J.Y. Wang, Biosens. Bioelectron. 25 (2010) 1248–1251.
[15] H.Y. Tsai, C.C. Wu, C.Y. Lee, E.P. Shih, J. Power Sources 194 (2009) 199–205.
[16] J.J. Sun, H.Z. Zhao, Q.Z. Yang, J. Song, A. Xue, Electrochim. Acta 55 (2010) 3041–3047.
[17] R.L. Vander Wal, T.M. Ticich, V.E. Curtis, Chem. Phys. Lett. 323 (2000) 217–223.
[18] C.X. Pan, Y.L. Liu, F. Cao, J.B. Wang, Y.Y. Ren, Micron 35 (2004) 461–468.
[19] L. Yuan, K. Saito, W. Hu, Z. Chen, Chem. Phys. Lett. 346 (2001) 23–28.
[20] C.P. Arana, I.K. Puri, S. Sen, Proc. Combust. Inst. 30 (2005) 2553–2560.
[21] S. Sen, I.K. Puri, Nanotechnology 15 (2004) 264–268.
[22] S. Naha, S. Sen, I.K. Puri, Carbon 45 (2007) 1702–1706.
[23] C. Dumas, A. Mollica, D. Feron, R. Basseguy, L. Etcheverry, A. Bergel, Electrochim. Acta 53 (2007) 468–473.
[24] C. Dumas, A. Mollica, D. Feron, R. Basseguy, L. Etcheverry, A. Bergel, Bioresour. Technol. 99 (2008) 8887–8894.
[25] T.H. Pham, P. Aelterman, W. Verstraete, Trends Biotechnol. 27 (2009) 168–178.
[26] C.P. Arana, M. Pontoni, S. Sen, I.K. Puri, Combust. Flame 138 (2004) 362–372.
[27] S. Naha, I.K. Puri, J. Phys. D: Appl. Phys. 41 (2008).
[28] S. Banerjee, S. Naha, I.K. Puri, Appl. Phys. Lett. 92 (2008).
[29] S. Naha, S. Sen, A.K. De, I.K. Puri, Proc. Combust. Inst. 31 (2007) 1821–1829.
[30] S. Mazumder, S. Ghosh, I.K. Puri, Proc. Combust. Inst. 33 (2011) 3351–3357.
[31] S.K. Aggarwal, I.K. Puri, AIAA J. 36 (1998) 1190–1199.
[32] A. Lock, S.K. Aggarwal, I.K. Puri, Proc. Combust. Inst. 32 (2009) 2583–2590.
[33] Z. He, S.D. Minteer, L.T. Angenent, Environ. Sci. Technol. 39 (2005) 5262–5267.
[34] L.T. Angenent, S. Sung, Water Res. 35 (2001) 1739–1747.
[35] S. Gunther, T. Hubschmarm, M. Rudolf, M. Eschenhagen, I. Roske, H. Harms, S. Muller, J. Microbiol. Methods 75 (2008) 127–134.
[36] R.S. Oremland, J.S. Blum, C.W. Culbertson, P.T. Visscher, L.G. Miller, P. Dowdle, F.E. Strohmaier, Appl. Environ. Microbiol. 60 (1994) 3011–3019.
[37] K. Bagramyan, N. Mnatsakanyan, A. Trchounian, Biochem. Biophys. Res. Commun. 306 (2003) 361–365.
[38] T. Sun, G. Wang, H. Liu, L. Feng, L. Jiang, D. Zhu, J. Am. Chem. Soc. 125 (2003) 14996–14997.
[39] H. Schulz, M. Leonhardt, H.J. Scheibe, B. Schultrich, Surf. Coat. Technol. 200 (2005) 1123–1126.
[40] S. Mazumder, J.O. Falkinham III, A.M. Dietrich, I.K. Puri, Biofouling 26 (2010) 333–339.
[41] A.V. Liopo, M.P. Stewart, J. Hudson, J.M. Tour, T.C. Pappas, J. Nanosci. Nanotechnol. 6 (2006) 1365–1374.
[42] S. Cheng, H. Liu, B.E. Logan, Environ. Sci. Technol. 40 (2006) 2426–2432.
[43] S. Cheng, H. Liu, B.E. Logan, Environ. Sci. Technol. 40 (2006) 364–369.
[44] H. Liu, S. Cheng, B.E. Logan, Environ. Sci. Technol. 39 (2005) 658–662.
[45] B. Logan, S. Cheng, V. Watson, G. Estadt, Environ. Sci. Technol. 41 (2007) 3341–3346.
[46] S. You, Q. Zhaoa, J. Zhang, J. Jiang, C. Wan, M. Dua, S. Zhaob, J. Power Sources 173 (2007) 172–177.
[47] K. Rabaey, P. Clauwaert, P. Aelterman, W. Verstraete, Environ. Sci. Technol. 39 (2005) 8077–8082.
[48] Y. Feng, H. Lee, X. Wang, Y. Liu, W. He, Bioresour. Technol. 101 (2010) 632–638.
[49] S. Srivastava, N.A. Kotov, Acc. Chem. Res. 41 (2008) 1831–1841.
[50] R.L. Vander Wal, L.J. Hall, Chem. Phys. Lett. 349 (2001) 178–184.
[51] MEPS International Ltd., N. America, All Products Stainless Steel Price Index (Grade 304), 2011, website, http://www.meps.co.uk/webcontent/StainlessNAComposite304.htm.
[52] W. Merchan-Merchan, A.V. Saveliev, L. Kennedy, W.C. Jimenez, Prog. Energy Combust. Sci. 36 (2010) 696–727.
[53] Y.A. Gorby, S. Yanina, J.S. McLean, K.M. Rosso, D. Moyles, A. Dohnalkova, T.J. Beveridge, I.S. Chang, B.H. Kim, K.S. Kim, D.E. Culley, S.B. Reed, M.F. Romine, D.A. Saffarini, E.A. Hill, L. Shi, D.A. Elias, D.W. Kennedy, G. Pinchuk, K. Watanabe, S. Ishii, B. Logan, K.H. Nealson, J.K. Fredrickson, PNAS 103 (2006) 11358–11363.
[54] K. Rabaey, N. Boon, M. Hofte, W. Verstraete, Environ. Sci. Technol. 39 (2005) 3401–3408.